IJASRM International Journal of Advanced Scientific Research and Management, Special Issue 4, ICAMA-18, Apr 2019
www.ijasrm.com
ISSN 2455-6378

Germanium oxide - doped magnesium oxide nanomaterial synthesized by green method and their characterization studies

A.Suba[1,4*], P.Selvarajan[2,4], J. Jebaraj Devadasan[3,4]

[1]Research scholar, Reg.No. 19132152132001, Department of Physics, Pope's College, Sawyerpuram, Thoothukudi-628251, Tamilnadu, India.

[2]Department of Physics, AditanarCollege of arts and science, Tiruchendur, Thoothukudi-628216, Tamilnadu, India

[3]PG & Research Department of Physics, Pope's College, Sawyerpuram,Thoothukudi-628251, Tamilnadu, India.
[4]Manonmaniam Sundaranar University, Abishekapatti, Tirunelveli-627012, Tamilnadu, India.

Abstract

This paper discusses in detail about the germanium oxide-doped magnesium oxide (GOMO) nanoparticles that were prepared by green synthesis. In this method, betel leaves were used for the preparation of GOMO nanomaterial. Green synthesis is an important method to prepare nanomaterials of varieties of undoped and doped samples and it is free from chemical contaminant. Leaf extract-based synthesis of metal oxide nanoparticles enables the production of non-toxic nanoparticles due to the availability of several photochemical and biological components that are advantageous for sensor and therapeutic applications. The prepared sample was utilised to analyse the crystal size and structure using powder X-ray diffraction (XRD). Optically, the prepared sample was examined using UV-visible spectroscopy. HRSEM analyses validate the shape, crystallinity, and particle size of the synthesised GeO_2 doped MgO nanoparticles. Elements including Ge, Mg, and O were found in the sample, according to the EDS investigations. The prepared sample's impedance studies are also examined

Keywords: *Germanium Oxide, Magnesium Oxide, HRSEM, EDS, Powder XRD, Impedamce*

1. Introduction

Nanotechnologies will make it possible for more effective manufacturing processes to generate a variety of multifunctional materials at low cost with less resource consumption and waste. But it's crucial to evaluate claims of probable environmental advantages over a material or product's whole lifespan, from production through use and disposal. We advise doing lifecycle analyses for applications of nanotechnologies [1-3]. As an alternative to chemical and physical procedures, green syntheses or green methods simply referred to the synthesis of metal NPs using plants, plant parts, or plant extracts. An emerging discipline in the combined realms of biotechnology and nanotechnology is called green synthesis, and it offers enormous economic and environmental advantages. Green synthesis has several drawbacks, such as a labor-intensive process and lack of repeatability, but it is crucial to use this strategy to develop dependable, sustainable, and environmentally friendly synthesis processes in order to prevent the development of undesired or dangerous byproducts. The green synthesis of NPs seeks to reduce waste production and adopt sustainable practises [4].

Scientists are quite concerned about metal oxides due to their better surface composition and large surface area. One of the most significant metal oxides is magnesium oxide (MgO), which has a variety of uses in the catalysis [5, 6, 7], refractory materials [8], paint [9], and superconducting industries [10], as well as in the biological, electrochemical, and medicinal areas [11]. Due to their unique characteristics, such as a high surface energy relative to their bulk counterparts, a large surface area to volume ratio, optical properties, and electrochemical properties, metal nanoparticles have a variety of uses in the biological, electrochemical, environmental,

medicinal, and environmental domains [12,13,14,15]. Magnesium oxide is crucial because it differs from bulk materials in a number of fundamental ways. Targeting several locations in biological systems, metal-based nanoparticles may also lessen the chance of developing drug resistance [17,18]. An inorganic substance with the chemical formula GeO2, germanium dioxide is also known as germanium (IV) oxide, germania, and salt of germanium [19]. It serves as the primary industrial source of germanium. In addition, when pure germanium comes into contact with ambient oxygen, it develops as a passivation layer. In the synthesis of additional germanium compounds as well as polyethylene terephthalate resin, germanium dioxide is utilised as a catalyst. Some phosphors and semiconductor materials are produced using it as a feedstock [20,21]. Both the amorphous and crystalline forms of germanium oxide are interesting due to their optical and electrical characteristics. Deep submicron technology is made possible by the high k interlayer dielectric material germanium oxide, which advances integrated circuit technology. It is particularly intriguing for high-frequency applications since it also possesses large carrier mobilities. Infrared spectroscopes employ germanium oxides because they are transparent to infrared light.GeO2 has a refractive index that is somewhat higher than SiO2's, is thermally stable, has a large band gap energy of 5 eV, a high dielectric constant, and is mechanically strong [22, 23]. MgO has a poor electrical conductivity and a high thermal conductivity. Comparing MgO to organic antimicrobial compounds, which have lower stability but stronger antibacterial action, has been a fascinating area of research in recent years [26]. By using green synthesis, germanium oxide doped magnesium oxide nanoparticles are created. Betel leaves are utilised in this process of green synthesis. Green synthesis has made considerable use of plant leaf extracts. As plants are generally available, secure to handle, and have a variety of metabolites that serve as reducing agents in the creation of nanoparticles, they include a large spectrum of bioactive phytochemicals. It has applications in a number of domains, including sensor, biological, and pharmacological ones [27]. Rosa floribunda charisma extract and its antioxidant, antiaging, and antibiofilm capabilities were used by Younis Inas et al. to create green magnesium nanoparticles [28]. Ikram et al. produced MgO nanostructures with graphene oxide doping for extremely effective dye degradation and antibacterial activity [29]. Effect of synthesis temperature on the morphological, optical, and electrical characteristics of MgO nanostructures has been shown by Sagadevan Suresh et al. [30]. Enhancing the antibacterial, cytotoxic, larvicidal, and repulsive properties of brown algae by the green production of magnesium oxide nanoparticles is a work by Fouda et al. [31]. For photocatalytic activity and antibacterial effectiveness, Khan Muhammad Isa et al. achieved green synthesis of magnesium oxide nanoparticles using Dalbergia sissoo extract [32]. Green production of magnesium oxide nanoparticles and its uses have been prepared by Abinaya et al. A critique [33]. Magnesium oxide nanoparticles (MgONps): green production, characterizations, and antibacterial activity have been established by Singh et al. [34]. The biological uses of phytoassisted production of magnesium oxide nanoparticles from Pterocarpus marsupium rox. b heartwood extract have been described by Ammulu Manne Anupama et al. [35]. Green production of Ni-doped magnesium oxide nanoparticles and its impact on photocatalysis have been established by Kulkarni Jeetendra et al. [36]. Using an aqueous extract of Sargassum wightii, Pugazhendhi Arivalagan et al. developed anticancer, antibacterial, and photocatalytic activities of green synthesised magnesium oxide nanoparticles (MgONPs) [37]. Magnesium oxide-Germanium dioxide Nanocomposite Powders with Biomimetic Synthesis and Antibacterial Properties have been developed by Avanzato et al. [38]. Synthesis of Germanium Oxide Nanoparticles in Low-Pressure Premixed Flames has been developed by Simanzhenkov et al. [39]. Rare-Earth Doped Germanium Oxide Glasses with Metallic Nanoparticles have been shown to exhibit Enhanced Photoluminescence and a planar waveguide by De Araujo et al. [40]. With the use of betel leaf extract, Palanisamy et al. have created green MgO nanoparticles for antibacterial activity [41]. From the reviews, it appears that green synthesis is not used to create germanium oxide nanoparticles. The green synthesis method will be used to create germanium oxide doped magnesium oxide nanoparticles. Characterising the synthesised sample is the primary goal of this work.

2. Materials and Methods

Sigma Alrich Company and Merck are the suppliers of Germanium oxide and magnesium nitrate, respectively. In Tamil Nadu, betel leaves are bought at the neighbourhood market. Separately, fresh betel leaves were added to deionized water. For 30 min. at 80°C, the mixtures were stirred using a magnetic stirrer. The extracts were subsequently filtered through a mesh and Whatman No. 1 filter paper to eliminate solid particles after being allowed to cool to room temperature.Germanium oxide powder was used as a doping agent and the extracts were mixed well for 3 hours at 30oC. A precipitate with a light-yellow hue developed and was filtered out. A muffle furnace was used to calcinate at 400°C for 12 hours. Figure 1 depicts the process flow for creating MgO nanoparticles doped with germanium oxide.

IJASRM
International Journal of Advanced Scientific Research and Management, Special Issue 4, ICAMA-18, Apr 2019
www.ijasrm.com
ISSN 2455-6378

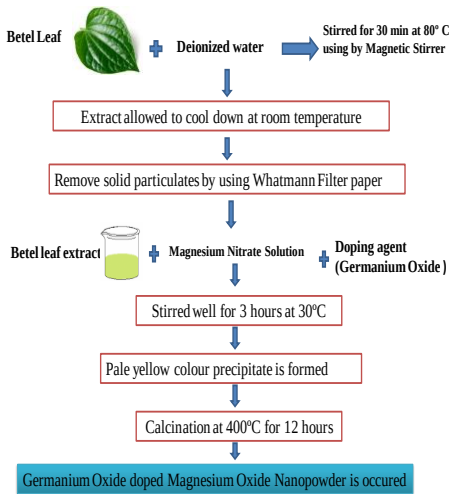

Fig.1: The flow chart for preparing GeO_2doped MgO nanoparticles

3. Results and Discussion

3.1 Structural characterization

The samples were analysed using an X-ray diffractometer (model: PAN Analytical Xpert- PRO) with Cu-K radiation (λ = 1.540) and 2θ values ranging from 10° to 85° in order to detect the crystal structure and phases in the manufactured products.The XRD pattern of Germanium Oxide doped MgO nanoparticles shows 2θ values at 25.69º, 37.77º, 42.7º, 58.57º, 62.14º, and 78.49° corresponding to the (hkl) planes at (101), (111), (200), (220), (311) and (222) respectively. All the observed peaks are matched well with JCPDS card number (No.075-0447).

GeO_2 doped MgO nanoparticles have a lattice parameter value of 4.231, which is somewhat different than the value for undoped MgO nanoparticles. GeO_2 in the sample is what causes the extra reflection peaks in the spectrum. The cubic structure of the MgO sample has been determined by XRD examination. Diffraction peaks were similar after doping, indicating a little amount of utilised dopant GeO2 that was undetectable. The Debye-Scherrer formula for particle size has been used to determine the average crystallite size.

$$D = \frac{K\lambda}{\beta cos\theta}, \qquad (1)$$

where K is a constant, equal to 0.9, β is the full width at half maximum, and λ is the X-ray wavelength, which is 1.5406Å. GeO_2 doped MgO nanoparticle crystallite size is 26.06 nm.

The calculated values of lattice constant (a), volume of unit cell (V), X-ray density (ρ_x), bulk density (ρ_b), and percentage of porosity (P) respectively are given in table 2.

The lattice constant which describes the spacing between adjacent unit cells in a crystal structure is calculated from d-spacing using the relation:

$$a = d(h^2 + k^2 + l^2)^{1/2} \qquad (2)$$

Where h, k, l are the miller indices of (200) plane. The volume of a cubic unit cell is calculated from lattice constant as:

$$V = a^3 \qquad (3)$$

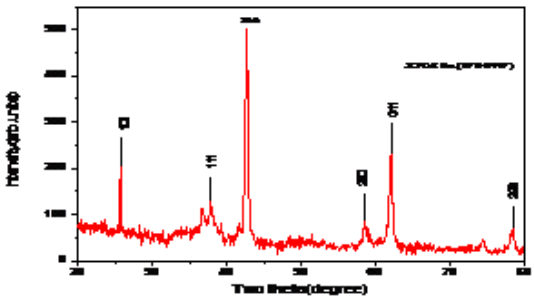

Figure 2. Powder XRD pattern of GeO_2 doped MgO Nanoparticles

Table1. Powder XRD data for GeO_2 doped MgO Nanoparticles

Two-theta (degrees)	d-spacing (Aº)	Relative Intensity (%)	hkl
25.69	0.14	30.55	101
37.77	0.29	18.35	111
42.71	0.39	100	200
58.54	0.29	1.37	220
62.14	0.34	43.06	311
78.49	0.59	9.58	222

The X-ray density depends on the molecular weight (M) and lattice constant of the sample. The value is calculated from the relation

$$\rho_x = \frac{8M}{Na^3} \qquad (4)$$

Where N is the Avogadro's number. The bulk density is calculated from the mass (m) and the dimensions of the pelletized sample using equation:

$$\rho_b = \frac{m}{\pi r^2 h} \qquad (5)$$

Where r is the radius and h is the thickness of the cubet. It is observed from table 2 that the bulk density is smaller than X-ray density. This explains the existence of pores in the material during formation and development of the material. The presence of pores is also confirmed from percentage of porosity. The percentage of porosity of the sample is calculated from X-ray density and bulk density using the relation:

$$P = (1 - \rho_b/\rho_x) \times 100 \qquad (6)$$

The value of porosity is high. So, in this sample, all the atoms are arranged in a regular pattern [42].

Table 2: Values of structural parameters for GeO_2 doped MgO nanoparticles

a (Å)	V $(Å)^3$	ρ_x (g/cm^3)	ρ_b (g/cm^3)	P (%)
4.231	75.74	4.56	2.27	50.21

IJASRM International Journal of Advanced Scientific Research and Management, Special Issue 4, ICAMA-18, Apr 2019
www.ijasrm.com
ISSN 2455-6378

A characteristic of solids called specific surface area measures the entire surface area of a substance per unit mass. Using the relationship between average crystallite size and X-ray density, the specific surface area is determined:

$$S = 6000/\rho_x D \quad (7)$$

$= 50.49X10^3$ m^2/g

Due to the particle's small size (nanoscale), the specific surface area is considerable, which improves the material's characteristics.

The following factors are used to calculate the dislocation density, which counts the number of dislocations in a unit volume of crystalline material:

$$\rho_D = \frac{1}{D^2} \quad (8)$$

$= 14.72X10^{-14}(m^{-2})$

The root mean square fluctuations of the lattice parameter across the crystallite as a result of the presence of defects and stress are measured as microstrain (the strain or deformation caused inside a crystal lattice rather than a bulk crystal). The Scherrer's relation allows for its calculation:

$$\varepsilon_s = \frac{\beta}{4\tan\theta} \quad (9)$$

The dislocation density and microstrain produced is large due to nanosize of the particles [43].

3.2 Optical characterization

The UV-visible transmission spectrum of GeO_2 doped MgO nanoparicles was recorded on a SHIMADZU UV-240 IPC spectrophotometer in the range of 200-900 nm. The prepared sample was directly placed in the spectrum was recorded and it is shown in the figure 3. From the results, the lower cut-off wavelength for the sample is observed to be at 230 nm and the percentage of transmission is noticed to be about 93% in the visible region. The peak at 268 nm indicates the confirmation of the formation of nanosized MgO particles and it is observed to be in good agreement with the reported value [44, 45].

The optical absorption coefficient (α) of GeO_2 doped MgO nanoparticles was determined using the relation

$$\alpha = [2.303 * log_{10}(1/T)]/d \quad (10)$$

where T is the transmittance and d is the sample holder's travel length. Figure 4 shows the wavelength vs absorbance coefficient curve for GeO_2 doped MgO nanoparticles. The absorption edge for GeO_2 doped MgO nanoparticles is determined to be 230 nm, and it is noted that the linear absorption coefficient is low in the visible range. Electronic transitions inside the samples cause absorption in the near UV range. Using the connection provided by Tauc, the optical band gap (Eg) was calculated from the spectrum and optical absorption coefficient (α) close to the absorption edge.

$$(\alpha h\vartheta)^n = A(h\vartheta - E_g), \quad (11)$$

where v is the frequency of the incoming photons, h is the Planck's constant, Eg is the optical band gap, and A is a proportional constant. Since the MgO sample has a straight band gap, n is equal to 2. In figure 5, Tauc's plot between $(\alpha hv)^2$ and h was created. The obtained value of optical band gap for MgO nanoparticles is 4.21 eV and this is observed to be low compared to the band gap of MgO nanoparticles. It is mentioned here that band gap of MgO nanoparticle is 5.45 eV[46].The lower band gap energy is certainly attributed to nano regime of MgO and it is due to the presence of 4-coordinated surface anions at the edges in the MgO nanoparticles whereas the bulk materials comprise 6-coordinated surface anions [47].

The extinction coefficient of the sample was calculated using the relation

$$K = \alpha\lambda/4\pi \quad (12)$$

where α is the linear absorption coefficient and λ is the wavelength of the light. The plot of photon energy dependence of extinction coefficient for sample is shown in the figure 6. The result indicates that the extinction coefficient is low in the visible region. Since the extinction coefficient of the sample is low of the order of 10^{-5}, the MgO nanopartilces can be used in optical applications. It is noticed that the extinction coefficient of the sample is high at the fundamental absorption in the UV region [48,49].

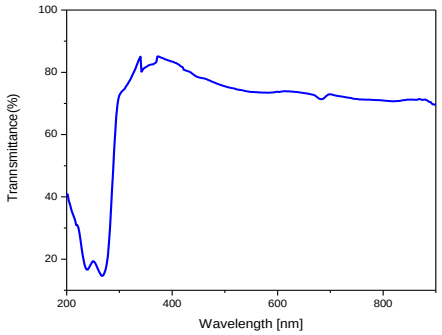

Fig.3 Transmittance spectrum of GeO_2 doped MgO Nanoparticles

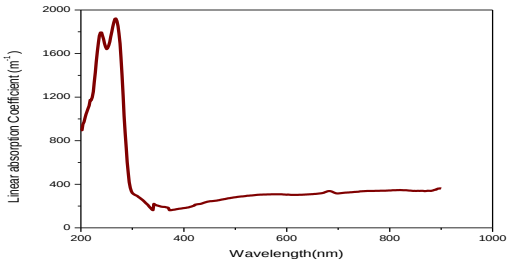

Fig.4Variation of absorption coefficient with wavelength for GeO_2 doped MgO nanoparticles

IJASRM
International Journal of Advanced Scientific Research and Management, Special Issue 4, ICAMA-18, Apr 2019
www.ijasrm.com
ISSN 2455-6378

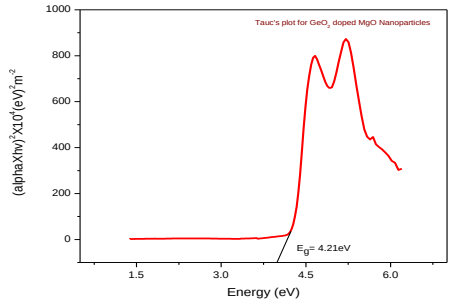

Fig.5 Tauc's plot for GeO_2 doped MgO nanoparticles

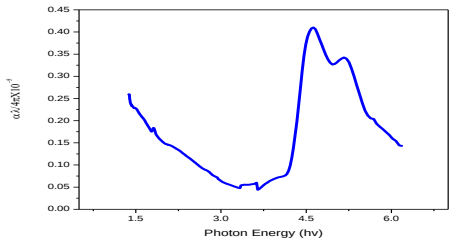

Fig.6 Variation of extinction coefficient with photon energy for GeO2 doped MgO Nanoparticles

Utilising the following relationship(R), reflectance and refractive index(n) values are calculated.

$$n = \left(\frac{1}{T} + \left(\frac{1}{T} - 1\right)\right) \quad (13)$$

$$R = (n-1)^2/(n+1)^2 \quad (14)$$

The plot of R and n against the wavelength are displayed in the figure 7 and 8 respectively. From figure 7 shown that the wavelength increases, the refractive index is decreases.

Using the following relation, the optical conductivity of GeO_2 doped MgO nanoparticles in SI units was calculated.

$$\sigma_{op} = \varepsilon_0 cn\alpha \quad (15)$$

where c is the speed of light in empty space, n is the refractive index, α is the linear absorption coefficient, and $\varepsilon_o$is the permittivity of empty space or vacuum. The following relation may be used to obtain the sample's optical conductivity value in Gaussian units:

$$\sigma_{op} = (1/4\pi\varepsilon_o)\varepsilon_o cn\alpha = (9 \times 10^9)\varepsilon_o cn\alpha \quad (16)$$

Since optical conductivity is a function of refractive index, the plots of optical conductivity versus refractive index for GeO_2 doped MgO nanoparticles are presented in the figure 9. The results reveal that the values of optical conductivity in SI units and Gaussian units linearly increases with increase of refractive index.

The complex dielectric constant of the sample can written as

$$\varepsilon^* = \varepsilon_r + j\varepsilon_i = (n + jK)^2, \quad (17)$$

where ε_r is the real part of dielectric constant, ε_i is the imaginary part of dielectric constant, n is refractive index and K is the extinction coefficient. The above relation can be written as

$$\varepsilon^* = \varepsilon_r + j\varepsilon_i = n^2 - K^2 + j2nK \quad (18)$$

And hence the real and imaginary parts of dielectric constant can be written as

$$\varepsilon_r = n^2 - K^2 \text{ and } \varepsilon_i = 2nK \quad (19)$$

The following formulas may be used to calculate the real and imaginary parts of the dielectric constant of GeO_2 doped MgO nanoparticles as a function of photon energy. Figure 10 displays the plot of the real portion of the dielectric constant for GeO_2 doped MgO nanoparticles as a function of photon energy. The real component is large around the fundamental absorption area.

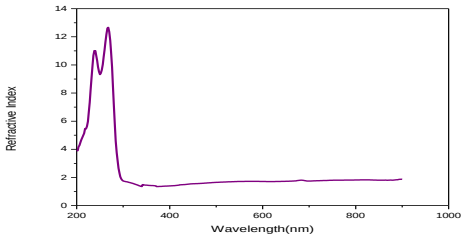

Fig.7 Variation of linear refractive index with wavelength for GeO2 doped MgO nanoparticles

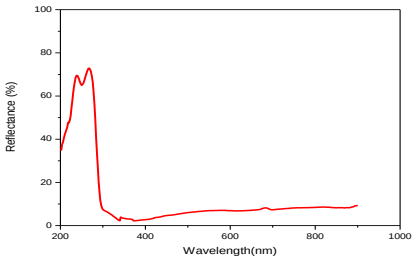

Fig.8 Reflectance Verses Wavelength of GeO_2 doped MgO nanoparticles

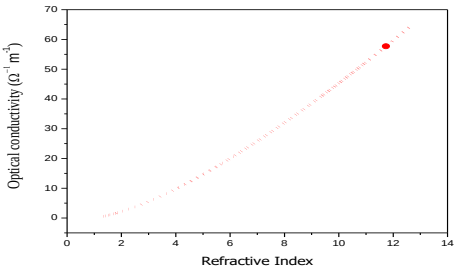

Fig.9 Plots of optical conductivity versus refractive index of GeO_2 doped MgO nanoparticles in SI units

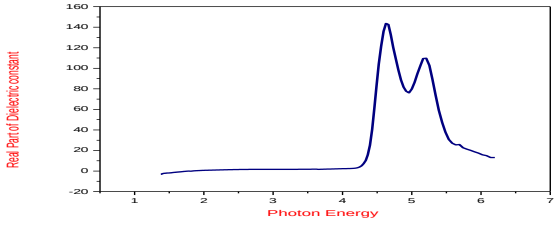

Fig.10 Variation of real part of dielectric constant with photon energy for GeO_2 doped MgO nanoparticles

IJASRM
International Journal of Advanced Scientific Research and Management, Special Issue 4, ICAMA-18, Apr 2019
www.ijasrm.com
ISSN 2455-6378

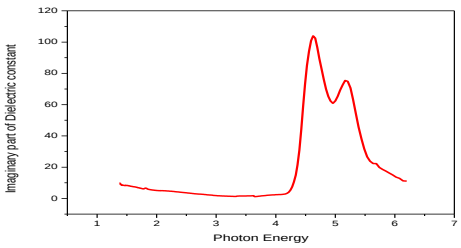

Fig.11 Variation of imaginary part of dielectric constant with photon energy for GeO2 doped MgO nanoparticles

3.3 HRSEM-EDX Analysis

A focussed electron beam is used to scan a sample in a scanning electron microscope (SEM) to create pictures of the material. With a magnification range that includes that of optical microscopy and extends to the nanoscale, the electrons interact with the atoms in the sample to produce a variety of signals that carry data on the surface topography and composition of the sample [50]. Using an HRSEM-FEI Quanta 200 MK II with an accelerating voltage of 1 to 30 kV and an EDX resolution of 136 eV, a research of GeO2 doped MgO nanomaterial was conducted. The Quanta 200F is a field emission gun (FEG) scanning electron microscope (SEM) that can also be used in environmental (ESEM) mode, which makes it possible to image things like biological materials without lysing cells due to a greater chamber pressure (0.1 to 27 mbar)[51]. The IIT Madras in Chennai provided the analysis for this article. Figure 12 displays high-resolution SEM pictures of the sample at various resolutions.The photos show that at 60,000 times their original size, the particles are spherical. Figure 13 displays the GeO2 doped MgO nanomaterial's observed EDX/EDS spectra. Different locations are concentrated during the EDS measurement, and the figure shows the appropriate peaks. Sharp peaks in the spectrum demonstrate the existence of Mg, O, and Ge elements. As a result, it is proven that Ge and O dopants are present in MgO nanomaterial. The values of nanoparticles are given below and are expressed in atomic weight percentage.

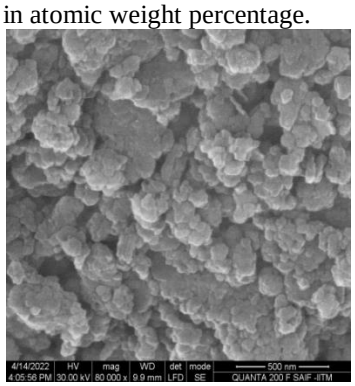

Fig. 12: Images of High Resolution Scanning Electron microscope of GeO_2 doped MgO Nanoparticles.

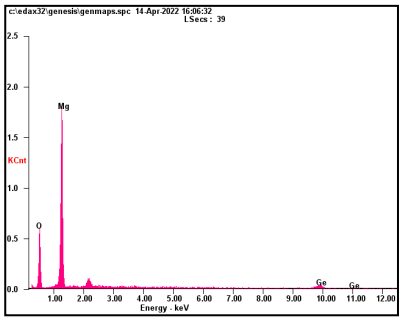

Fig. 13: EDX spectrum of Germanium Oxide doped Magnesium Oxide nanoparticles

3.4 Impedance Analysis

The combination of reactance and resistance is called as impedance denoted by Z. Its unit is Ω. An electric component which opposition of change in current is called reactance and an electric component which opposition of flow of current is called resistance. Impedance affects the generation of current through the electric circuit. The impedance curves for GOMO sample are shown in figure 14. It is noted that Z' exhibits a high value at a lower frequency, followed by a fall and a rise in frequency that superimposes at the highest frequency value. The rising Z' indicates a stronger interfacial polarisation effect from the previously described dielectric system. As a result of the release in the space charge, Z' exhibits a fall at high frequency values, confirming the enhanced ac conductivity at those frequencies. As Z'', the imaginary component of impedance, equals CR2, it produces resistance and a shift in frequency.

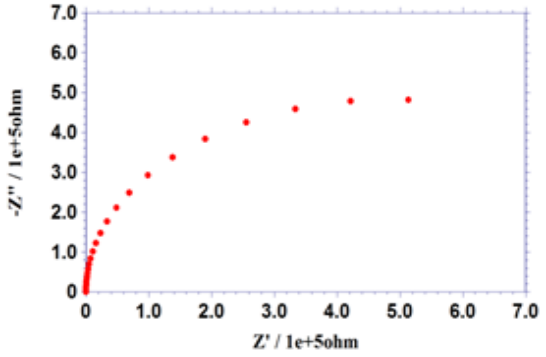

Figure 14: The impedance curves for GOMO sample

5. Conclusions

Germanium oxide, magnesium nitrate, and betel leaf extract were used to create the GeO2 doped magnesium oxide (GOMO) nanomaterial using a green manufacturing process. The large reflection peaks in the powder XRD pattern show that the sample is a nanomaterial. The sample was discovered to have a cubic crystal structure, and the crystal structure was unaltered by the doping of GeO_2. The average particle size of the sample was determined by a Powder XRD investigation to be

26.06 nm.The UV-visible spectrum is used to analyse the optical characteristics of the GOMO nanomaterial, and linear optical parameters have been assessed. At various resolutions, HRSEM pictures of the sample have been acquired; the images show that the sample comprises particles with spherical and elongated forms. The Mg, O, and Ge elements that are present in the sample are represented by a number of strong peaks in the EDX spectrum. The sample exhibits the characteristics of an insulating substance, as seen by its impedance spectrum.

Acknowledgments
The authors are thankful to the management of Aditanar College of arts and science, Tiruchendur, Pope's College in Sawyerpuram for their support in carrying out the research work. Also the authors acknowledge the research centers like STIC (Cochin University), SAIF (IIT, Madras), Alagappa University (Karaikudi), V.O.Chidambaram College (Thoothukudi) for getting the research data of the sample..

Reference

1. Philip S. Anton, Richard Silberglitt, James Schneider, The Global Technology Revolution:Bio/Nano/Materials Trends and their Synergies with Information Technology by 2015.
2. A.H. Arnall, Future Technologies, Today's Choices: Nanotechnology, Artificial Intelligence and Robotics. Department of Environmental Science and Technology Environmental Policy and Management Group, Faculty of Life Sciences, Imperial College London, University of London. (2003)
3. J. Arvai, R. Gregory & T. McDaniels, Testing a structured decision-aiding approach: value-focused thinking for deliberative risk communication, Risk Analysis 21(2001), pp.1065–1076,
4. G.Dercz, K.Prusik, L.Pajak, R.Pielaszek, J.J.Malinowski, W.Pudło, Structure Studies on Nanocrystalline Powder of MgO Xerogel Prepared by the Sol-Gel Method. *Mater. Sci.* 27(2009)201–207
5. S.H. Liang, I.D. Gay, A carbon-13 solid-state NMR study of the chemisorption and decomposition of ethanol on magnesium oxide, JCatal 101.2, (1986), pp.293–300,
6. H. Tsuji, F.Yagi, H. Hattori, H. Kita, Self-condensation of n butyraldehyde over solid base catalysts, J Catal 148(2) (1994), pp.759–770,
7. M.Y. Nassar, T.Y.Mohamed, I.S.Ahmed, I.Samir, MgO Nanostructure via a Sol-Gel Combustion Synthesis Method Using Different Fuels: An Efficient Nano-Adsorbent for the Removal of Some Anionic Textile Dyes. *J. Mol. Liq.* 225(2017)730–740.
8. A. Bhargava, J.A. Alarco, I.D. Mackinnon, D. Page, A. Ilyush-echkin, Synthesis and characterisation of nanoscale magnesium oxide powders and their application in thick films of Bi_2 Sr_2 $CaCu_2$ O_8, Mater Lett 34(3–6) (1998), pp.133–142,
9. Y.S. Yuan, S.S. Wang, Solid-state processing and phase development of bulk (MgO)w/BPSCCO high-temperature superconducting composite, J Mater Res 11(1) (1996), pp.8–1,
10. PD Yang, CM Lieber, Nanorod-superconductor composites: a pathway to high critical current density materials, Science 273 (1996), pp.1836–1849,
11. J. Kaur, J. Singh, M. Rawat, An efficient and blistering reduction of 4-nitrophenol by green synthesized silver nanoparticles, SN Appl Sci 1 (2019), 1060,
12. J. Singh, V. Kumar, S.S. Jolly, K.H. Kim, M. Rawata, D. Kukkara, Y.F. Tsange Biogenic synthesis of silver nanoparticles and its photocatalytic applications for removal of organic pollutants in water, J Industr Eng Chem 80 (2019), pp.247–257,
13. J. Singh, A. Mehta, M. Rawata, S. Basub, Green synthesis of silver nanoparticles using sun dried tulsi leaves and its catalytic application for 4-Nitrophenol reduction, J Environ Chem Eng 6 (2018), pp.1468–1474,
14. J. Singh, P. Kukkar, H. Sammi, M. Rawat, G. Singh, D. Kukkar, Enhanced catalytic reduction of 4-nitrophenol and congo red dye By silver nanoparticles prepared from Azadirachta indica leaf extract under direct sunlight exposure, Particul Sci Technol, (2017),
15. P.B.Devaraja, D.N.Avadhani, S.C.Prashantha, H.Nagabhushana, S.C.Sharma, B.M.Nagabhushana, H.P.Nagaswarupa, Synthesis, Structural and Luminescence Studies of Magnesium Oxide Nanopowder. *Spectrochim. Acta Part Mol. Biomol. Spectrosc.* 2014;118:847–851.
16. M. Rawat, J. Singh, J. Singh, C. Singh, A. Singh, D. Kukkar, S. Kumar, Synthesis of Cu and Ce-doped ZnO nanoparticles: crystallographic, optical, molecular, morphological and magnetic studies, Mater Sci 35(2) (2017),
17. R.S. Varma, Greener approach to nanomaterials and their sustainable applications, Curr Opin Chem Eng 1, (2012), pp.123–128,
18. A.Mahshad, J.Mona, R.Alimorad, Simple and Economical Method for the Preparation of MgO Nanostructures with Suitable Surface Area. *Iran. J. Chem. Chem. Eng.* 33(2014)21–28.
19. US Patent Application for Esterification catalysts Patent Application, patents.justia.com. Retrieved 2018-12-05.
20. Thiele, K. Ulrich, The Current Status of Catalysis and Catalyst Development for the Industrial Process of Poly(ethylene terephthalate) Polycondensation, International journal of polymeric Materials, 50(3) (2001), pp.387-394,
21. J.P.Singh, K.H. D. Chae, Ferromagnetism of Magnesium Oxide. *Condens. Matter*. 2017;2:36
22. S. Zhang, B.Yin, Y. Jiao, Y. Liu, X. Zhang, F. Qu, A.Umar, and X. Wu, Ultralong germanium oxide nanowires: Structures and optical properties, Journal of alloys and compounds 606 (2014), pp.149-153,
23. C. V. Ramana, G. Carbajal-Franco, R. S. Vemuri, I. B. Troitskaia, S. A. Gromilov, and V. V. Atuchin, Optical properties and thermal stability of germanium oxide (GeO2) nanocrystals with α-quartz structure, Materials Science and Engineering: B 174, no. 1-3 (2010), pp.279-284.
24. A. Chiasera, C. Macchi, S. Mariazzi, S. Valligatla, Lorenzo Lunelli, Cecilia Pederzolli, D. N. Rao, A. Somoza, R. S. Brusa, and M. Ferrari, CO2 Laser irradiation of GeO2 planar waveguide fabricated by RF-sputtering, OpticalMaterialsExpress3,no. 9 (2013),pp.1561-1570,

25. C.H. Hsu, J.S. Lin, Y.D. He, S.F. Yang, P.C. Yang, and W.S. Chen, Optical, electrical properties and reproducible resistance switching of GeO_2 thin films by sol–gel process, Thin Solid Films 519, no. 15 (2011), pp. 5033-5037.
26. Y.Ding, G.Zhang, H.Wu, B.Hai, L.Wang, Y.Qian, Nanoscale Magnesium Hydroxide and Magnesium Oxide Powders: Control over Size, Shape, and Structure via Hydrothermal Synthesis. *Chem. Mater*. 13(2001)435–440.
27. J. Jeevanandam, Y. San Chan, and M.K. Danquah, Biosynthesis and characterization of MgO nanoparticles from plant extracts via induced molecular nucleation, New Journal of Chemistry 41.7 (2017), pp. 2800-2814,
28. S.Rukh, A.H.Sofi, M.A.Shah, S.Yousuf, Antibacterial Activity of Magnesium Oxide Nanostructures Prepared by Hydrothermal Method. *Asian J. Nanosci. Mater*. 1999;2:425–430.
29. A.V.Varma, A.S.Mukasyan, A.S Rogachev, K.V.Manukyan, Solution Combustion Synthesis of Nanoscale Materials. *Chem. Rev.* 116(2016)14493–14586
30. K.V.Rao, C.S.Sunandana, Structure and Microstructure of Combustion Synthesized MgO Nanoparticles and Nanocrystalline MgO Thin Films Synthesized by Solution Growth Route. *J. Mater. Sci.* 43(2008)146–154.
31. A.Ranjan, S.S.Dawn, J.Jayaprabakar, N.Nirmala, K.Saikiran, S.Sai Sriram, Experimental Investigation on Effect of MgO Nanoparticles on Cold Flow Properties, Performance, Emission and Combustion Characteristics of Waste Cooking Oil Biodiesel. *Fuel.* 220(2018)780–791.
32. D.Kumar, L.S.R.Yadav, K.Lingaraju, K.Manjunath, D.Suresh, D. Prasad, H.Nagabhushana, S.C.Sharma, H.R.Naika, Chikkahanumantharayappa et al. Combustion Synthesis of MgO Nanoparticles Using Plant Extract: Structural Characterization and Photoluminescence Studies. *AIP Conf. Proc.* 1665(2015)050145.
33. J.Suresh, R.Yuvakkumar, M.Sundrarajan, S.I.Hong, Green Synthesis of Magnesium Oxide Nanoparticles. *Adv. Mater. Res.* 952(2014)141–144.
34. [34] Singh, A., Joshi, N.C. and Ramola, M., 2019. Magnesium oxide nanoparticles (MgONps): green synthesis, characterizations and antimicrobial activity. Research Journal of Pharmacy and Technology, 12(10), pp.4644-4646.
35. M.Vergheese, S.K.Vishal, Green Synthesis of Magnesium Oxide Nanoparticles Using Trigonella Foenum-Graecum Leaf Extract and Its Antibacterial Activity. *J. Pharmacogn Phytochem.* 7(2018)1193–1200.
36. Kulkarni J, Ravishankar R, Nagabhushana H, Ananthraju KS, Basavraj RB, Renuka L. Green synthesis of Ni-doped magnesium oxide nanoparticles and its effect on photo catalysis. Indian Journal of Advances in Chemical Science S1. 2016;64:67.
37. Pugazhendhi, A., Prabhu, R., Muruganantham, K., Shanmuganathan, R. and Natarajan, S., 2019. Anticancer, antimicrobial and photocatalytic activities of green synthesized magnesium oxide nanoparticles (MgONPs) using aqueous extract of Sargassum wightii. Journal of Photochemistry and Photobiology B: Biology, 190, pp.86-97.
38. Avanzato CP, Follieri JM, Banerjee IA, Fath KR. Biomimetic synthesis and antibacterial characteristics of magnesium oxide—germanium dioxide nanocomposite powders. Journal of composite materials. 2009 Apr;43(8):897-910.
39. Simanzhenkov V, Ifeacho P, Wiggers H, Knipping J, Roth P. Synthesis of germanium oxide nanoparticles in low-pressure premixed flames. Journal of Nanoscience and Nanotechnology. 2004 Jan 1;4(1-2):157-61.
40. De Araújo CB, Kassab LR. Enhanced photoluminescence and planar waveguide of rare-earth doped germanium oxide glasses with metallic nanoparticles. InGlass Nanocomposites 2016 Jan 1 (pp. 131-144). William Andrew Publishing.
41. Palanisamy G, Pazhanivel T. Green synthesis of MgO nanoparticles for antibacterial activity. International research journal of engineering and technology. 2017 Aug 4;4(9):137-41.
42. Chand P, Gaur A, Kumar A. Structural and optical properties of ZnO nanoparticles synthesized at different pH values. Journal of alloys and compounds. 2012 Oct 25;539:174-8.
43. Cullity, Bernard Dennis. Elements of X-ray Diffraction. Addison-Wesley Publishing, 1956.
44. Aslam M, Fu L, Su M, Vijayamohanan K, Dravid VP, Novel one-step synthesis of amine-stabilized aqueous colloidal gold nanoparticles. Journal of materials Chemistry, 14(12), 1795-1797, 2004.
45. Somanathan, Thirunavukkarasu, Vemula Mohana Krishna, Velautham Saravanan, Raju Kumar, Randhir Kumar, MgO nanoparticles for effective uptake and release of doxorubicin drug: pH sensitive controlled drug release, Journal of Nanoscience and Nanotechnology 16, 9, 9421-9431, 2016.
46. Tauc J, Optical properties and electronic structure of amorphous Ge and Si. Materials Research Bulletin, 3(1), 37-46, 1968.
47. G.Sharma, R.Soni, N.D.Jasuja, Phytoassisted Synthesis of Magnesium Oxide Nanoparticles with Swertia Chirayaita. *J. Taibah Univ. Sci.* 11(2017)471–477.
48. Berger T, Sterrer M, Stankic S, Bernardi J, Diwald O, Knozinger E, Trapping of photogenerated charges in oxide nanoparticles, Materials Science and Engineering: C. 25, 664-668,2005.
49. Tandon SP, Gupta JP, Diffuse reflectance spectrum of cuprous oxide. physica status solidi (b), 37(1), 43-45, 1969.
50. P.Murkute, H.Ghadi, S.Patil, H.Rawool, S.Pandey, S.Chakrabarti, Emerging Material Zinc Magnesium Oxide Based Nanorods: Growth Process Optimization and Sensor Application towards Humidity Detection. *Sens. Actuators Chem.* 256(2018)204–216..
51. Y.Tao, X.Cao, Y.Peng, Y.Liu, A Novel Cataluminescence Gas Sensor Based on MgO Thin Film. *Sens. Actuators Chem.* 148(2010)292–297.